

The Hercules stream as seen by APOGEE-2 South

Jason A. S. Hunt,^{1★} Jo Bovy,^{1,2†} Angeles Pérez-Villegas,³ Jon A. Holtzman,⁴
Jennifer Sobeck,⁵ Drew Chojnowski,⁴ Felipe A. Santana,⁶ Pedro A. Palicio,^{7,8}
Christopher Wegg,³ Ortwin Gerhard,³ Andrés Almeida,⁹ Dmitry Bizyaev,^{10,11}
Jose G. Fernandez-Trincado,^{12,13} Richard R. Lane,¹⁴ Penélope Longa-Peña,¹⁵
Steven R. Majewski,¹⁶ Kaike Pan¹⁰ and Alexandre Roman-Lopes¹⁷

¹Dunlap Institute for Astronomy and Astrophysics, University of Toronto, 50 St. George Street, Toronto, ON M5S 3H4, Canada

²Department of Astronomy and Astrophysics, University of Toronto, 50 St. George Street, Toronto, ON M5S 3H4, Canada

³Max-Planck Institut für Extraterrestrische Physik, Gießenbachstraße, D-85741 Garching, Germany

⁴Department of Physics and Astronomy, New Mexico State University, Las Cruces, NM 88003-8001, USA

⁵Department of Astronomy, Box 351580, University of Washington, Seattle, WA 98195, USA

⁶Departamento de Astronomía, Universidad de Chile, Av. Libertador Bernardo O'Higgins 1058, Santiago de Chile, Chile

⁷Instituto de Astrofísica de Canarias, E-38205 La Laguna, Tenerife, Spain

⁸Dpto. Astrofísica, Universidad de La Laguna, E-38206 La Laguna, Tenerife, Spain

⁹Instituto de Investigación Multidisciplinario en Ciencia y Tecnología, Universidad de La Serena, Benavente 980, La Serena, Chile

¹⁰Apache Point Observatory and New Mexico State University, PO Box 59, Sunspot, NM 88349-0059, USA

¹¹Sternberg Astronomical Institute, Moscow State University, 119992 Moscow, Russia

¹²Departamento de Astronomía, Universidad de Concepción, Casilla 160-C, Concepción, Chile

¹³Institut Utinam, CNRS UMR6213, Univ. Bourgogne Franche-Comté, OSU THETA, Observatoire de Besançon, BP 1615, F-25010 Besançon Cedex, France

¹⁴Instituto de Astrofísica, Pontificia Universidad Católica de Chile, Av. Vicuña Mackenna 4860, 782-0436 Macul, Santiago, Chile

¹⁵Unidad de Astronomía, Universidad de Antofagasta, Avenida Angamos 601, Antofagasta 1270300, Chile

¹⁶Department of Astronomy, University of Virginia, PO Box 400325, Charlottesville, VA 22904-4325, USA

¹⁷Departamento de Física, Facultad de Ciencias, Universidad de La Serena, Cisternas 1200, La Serena, Chile

Accepted 2017 October 23. Received 2017 October 23; in original form 2017 September 8

ABSTRACT

The Hercules stream is a group of comoving stars in the solar neighbourhood, which can potentially be explained as a signature of either the outer Lindblad resonance (OLR) of a fast Galactic bar or the corotation resonance (CR) of a slower bar. In either case, the feature should be present over a large area of the disc. With the recent commissioning of the APOGEE-2 Southern spectrograph we can search for the Hercules stream at $(l, b) = (270^\circ, 0)$, a direction in which the Hercules stream, if caused by the bar's OLR, would be strong enough to be detected using only the line-of-sight velocities. We clearly detect a narrow, Hercules-like feature in the data that can be traced from the solar neighbourhood to a distance of about 4 kpc. The detected feature matches well the line-of-sight velocity distribution from the fast-bar (OLR) model. Confronting the data with a model where the Hercules stream is caused by the CR of a slower bar leads to a poorer match, as the corotation model does not predict clearly separated modes, possibly because the slow-bar model is too hot.

Key words: Galaxy: bulge – Galaxy: disc – Galaxy: fundamental parameters – Galaxy: kinematics and dynamics – solar neighbourhood – Galaxy: structure.

1 INTRODUCTION

It has been known for considerable time that the Milky Way is a barred galaxy, initially inferred from observations of gas kinematics

(e.g. de Vaucouleurs 1964), and later confirmed by infrared photometry (e.g. Blitz & Spergel 1991). However, some of the fundamental parameters of the bar have not been fully determined, in particular its length, mass, pattern speed and angle with respect to the Sun–Galactic Centre line remain the subject of debate. This is primarily owing to the high levels of dust extinction present in the Galactic plane, especially when looking towards the inner Galaxy, and because the structure and kinematics of the bar and/or bulge region is

* E-mail: jason.hunt@utoronto.ca

† Alfred P. Sloan Fellow.

highly complex (e.g. Cabrera-Lavers et al. 2008; McWilliam & Zoccali 2010; Nataf et al. 2010; Ness et al. 2016; Williams et al. 2016; Portail et al. 2017b).

However, as an alternative to direct observation, we are able to infer properties of the bar from its effect on the orbits of stars further out in the Galaxy, especially those strongly affected by resonant interactions. Specifically, a rotating galactic bar has three fundamental resonances; the corotation resonance (CR), where $\Omega_\phi = \Omega_b$, and the inner (ILR) and outer (OLR) Lindblad resonances such that

$$\Omega_b = \Omega_\phi \pm \frac{1}{2}\Omega_R, \quad (1)$$

where Ω_b is the pattern speed of the bar and Ω_ϕ and Ω_R are the tangential and radial orbital frequencies. Dehnen (2000) proposed that the Hercules stream, a well-known feature in the kinematics of the solar neighbourhood, is caused by the OLR of the bar. To reproduce the observed kinematics, this explanation requires the OLR to be just inside the solar circle, with a bar pattern speed of around 1.85 times the local circular frequency. Note that while there are other possible explanations for Hercules, e.g. a moving group with a common birthplace within the disc, or the signature of a merger, the fact that it is comprised of old and late-type stars (e.g. Dehnen 1998) and spans a range of ages and metallicities (e.g. Famaey et al. 2005; Bensby et al. 2007; Bovy & Hogg 2010) argues for a dynamical origin. For this explanation Dehnen (2000) found the constraint $\Omega_b = (1.85 \pm 0.05) \times \Omega_0$, or $\Omega_b = 53 \pm 3 \text{ km s}^{-1} \text{ kpc}^{-1}$ for $\Omega_0 = 28.5 \text{ km s}^{-1} \text{ kpc}^{-1}$. This is in agreement with later work. For example, Minchev, Nordhaus & Quillen (2007) find $\Omega_b = (1.87 \pm 0.04) \times \Omega_0$ with an analysis of the Oort constants, and Minchev et al. (2010) find $\Omega_b = (1.82 \pm 0.07) \times \Omega_0$.

Antoja et al. (2014) use data from the Radial Velocity Experiment (RAVE; Steinmetz et al. 2006) to trace Hercules between Galactic radii $R = 7.8\text{--}8.6 \text{ kpc}$ (assuming the Sun to be located at $R_0 = 8.05 \text{ kpc}$). They find best-fitting values of $\Omega_b = (1.89 \pm 0.08) \times \Omega_0$, or $\Omega_b = 56 \pm 2 \text{ km s}^{-1} \text{ kpc}^{-1}$ for $\Omega_0 = 29.5 \text{ km s}^{-1} \text{ kpc}^{-1}$ under the assumption that the Hercules stream is caused by the OLR. Monari et al. (2017b) use data from the Large Sky Area Multi-Object Fibre Spectroscopic Telescope (LAMOST; Zhao et al. 2012) combined with data from the Tycho-Gaia Astrometric Solution (Gaia Collaboration 2016b) to trace the Hercules stream in the direction of the Galactic anticentre, up to a distance of 0.8 kpc. They find good agreement with the values from Antoja et al. (2014). These works show that the RAVE and LAMOST data are consistent with Hercules being caused by the OLR of the bar, and the measured pattern speeds put an upper limit on the length of the bar, which cannot extend past corotation (e.g. Contopoulos 1980). If Hercules is caused by the OLR, the bar is expected to end around 3–3.5 kpc from the Galactic Centre.

However, some recent studies of the bar favour a notably longer (e.g. Wegg, Gerhard & Portail 2015) and slower bar (e.g. Portail et al. 2017a). This is at odds with the interpretation of Hercules as a resonance feature of the OLR because in this scenario the OLR is a few kpc outside the solar circle. For example, in Pérez-Villegas et al. (2017), for a bar with half length $\sim 5 \text{ kpc}$ and pattern speed $\Omega_b = 39 \text{ km s}^{-1} \text{ kpc}^{-1}$, the OLR is located at $R \sim 10.5 \text{ kpc}$, and cannot be responsible for the Hercules stream. However, it is worth noting that an OLR like feature has been observed by Liu et al. (2012) at 10–11 kpc, which is consistent with this model. If the bar does extend to $\sim 5 \text{ kpc}$, then an alternate explanation is needed for the Hercules stream.

Pérez-Villegas et al. (2017) show that a 5 kpc bar in an N -body model is also able to reproduce the Hercules stream in the solar neighbourhood via a different mechanism, where stars orbiting the bar's Lagrange points L_4 and L_5 move outwards from corotation, which occurs at $R = 6 \text{ kpc}$, and reach the solar neighbourhood. In this model, the Hercules stream will be stronger within the solar radius, and should disappear a few hundred parsecs further from the centre. This is in contrast with the fast-bar model, where the Hercules stream should extend further beyond the solar radius (e.g. Bovy 2010). In the near future, the European Space Agency's *Gaia* mission (Gaia Collaboration 2016a) will enable us to probe much further from the solar neighbourhood, and potentially trace the extent of Hercules, determining which resonance is responsible. However, Bovy (2010) showed that in specific directions ($250^\circ < l < 290^\circ$), line-of-sight velocities alone are enough to observe Hercules if it is caused by the OLR, because in these directions the Hercules feature is well separated from the main mode of the velocity distribution along the direction that projects on to the line of sight.

The Sloan Digital Sky Survey IV (SDSS-IV; e.g. Blanton et al. 2017), Apache Point Observatory Galactic Evolution Experiment (APOGEE; Majewski et al. 2016, 2017) has provided high-resolution spectroscopic data for around 150 000 stars in the Northern hemisphere during its first phase, APOGEE-1 (Holtzman et al. 2015). Now, as part of its second phase, APOGEE-2, which includes a second spectrograph in the Southern hemisphere, APOGEE-2S, will extend APOGEE's coverage across the sky. The line-of-sight $(l, b) = (270^\circ, 0)$ is one of the first fields observed during the commissioning of the APOGEE-2S spectrograph, which enables us to look for the Hercules stream at the line of sight identified in Bovy (2010) as having a strong feature.

This paper is constructed as follows. In Section 2, we discuss our treatment of the data and the resulting velocity distribution. In Section 3, we present the model predictions for this line of sight from both the fast-bar model, and the slow-bar model from Pérez-Villegas et al. (2017). In Section 4, we compare the models with the data. In Section 5, we discuss the implications of the detection and look forward to future data.

2 OBSERVED FEATURE

We use spectroscopic data from the field centred on $(l, b) = (270^\circ, 0)$ taken during commissioning of the APOGEE-2 Southern spectrograph installed at the 2.5 m du Pont telescope (Bowen & Vaughan 1973) at Las Campanas Observatory. This spectrograph is almost an exact clone of the APOGEE spectrograph installed at the 2.5 m Sloan Foundation telescope (Gunn et al. 2006) and described in Wilson et al. (2010) and Wilson et al. (in preparation). The target selection is described in Zasowski et al. (2017). A fully customised reduction pipeline for the APOGEE-2S spectrograph is not yet available and we have therefore processed the spectra using the existing APOGEE reduction (Nidever et al. 2015) and stellar-parameter (ASPCAP; García Pérez et al. 2016) pipelines. Like the original APOGEE spectrograph, the APOGEE-2S spectrograph has 300 fibres and the data for the $(l, b) = (270^\circ, 0)$ field contain 262 stars (with 35 fibres assigned to observe the sky, two unmapped fibres and one with bad pixels).

Because this is the first application of the existing pipeline to data from the new spectrograph, we examine all the spectra and their radial velocity template fits by eye to remove low signal-to-noise ratio spectra and prevent bad template matching. We then run these spectra through the reduction and stellar-parameters pipeline

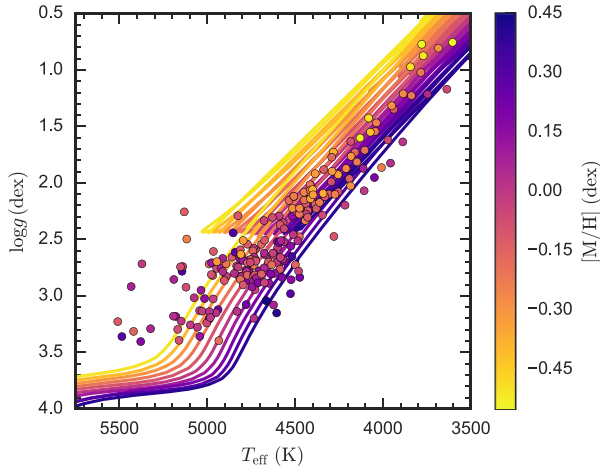


Figure 1. T_{eff} versus $\log g$ colour-coded by overall metallicity for the giant stars in the $(l, b) = (270^\circ, 0)$ field, overlaid on a small number of PARSEC isochrones for an age of 5 Gyr, colour-coded by the same metallicity scale.

to determine line-of-sight velocities v_{los} , effective temperature T_{eff} , surface gravity $\log g$ and the overall metallicity $[M/H]$. Other parameters ($[C/M]$, $[N/M]$, $[\alpha/M]$, ξ) are simultaneously fit by the pipeline, but we will ignore them for the time being. Our main use of the stellar parameters is to infer distances.

We correct the line-of-sight velocities using the solar motion from Bovy et al. (2012, 2015); because the observed field is small, we apply this correction as a constant correction of -24 km s^{-1} and v_{los} from here on refers to the corrected value. Note that towards $(l, b) = (270^\circ, 0)$ only the tangential component V_\odot of the solar motion matters. Applying a different solar motion would simply shift all of the line-of-sight velocities by a constant without changing the shape of the distribution of line-of-sight velocities.

We then select giants by requiring $\log g \leq 3.5$ and only consider stars with $-200 \leq v_{\text{los}} \leq 200 \text{ km s}^{-1}$ to remove outliers and possible halo stars. The remaining sample consists of 218 giant stars. Fig. 1 shows T_{eff} versus $\log g$ colour-coded by metallicity $[M/H]$ for these 218 stars, overlaid on a small number of PARSEC isochrones (Bressan et al. 2012) for an age of 5 Gyr, for illustration. Even though the data were only run through preliminary versions of the reduction pipelines, the stellar parameters follow the expected behaviour as a function of $(T_{\text{eff}}, \log g, [M/H])$ along the giant branch. Note that the full calibrations are not yet available for APOGEE-2S, thus this version of the pipeline uses the raw ASPCAP output, which produces reliable $[M/H]$ and T_{eff} , but can show an offset in $\log g$ of 0.2–0.3 dex relative to the asteroseismic gravities for giants.

Fig. 2 shows the distribution of line-of-sight velocities for the full sample. This distribution displays a clearly bimodal distribution. This structure is qualitatively what we expect to see for the Hercules stream, which is located around $V = -50 \text{ km s}^{-1}$ in the solar neighbourhood. The data prefer a double Gaussian fit over a single Gaussian fit at a significance of 4.8σ , although note that neither mode is expected to be Gaussian in nature.

We also wish to test how the Hercules feature changes with distance from the Sun. To split our sample in different distance bins, we estimate distances for the stars in our sample using the isochrone fitting code UNIDAM (Mints & Hekker 2017). UNIDAM estimates distances from the available stellar parameters (T_{eff} , $\log g$ and $[M/H]$), and from the J , H , K_s magnitudes, by comparing the data with PARSEC 1.2S isochrones in a Bayesian manner. UNIDAM fails for three stars not already excluded by earlier cuts, providing

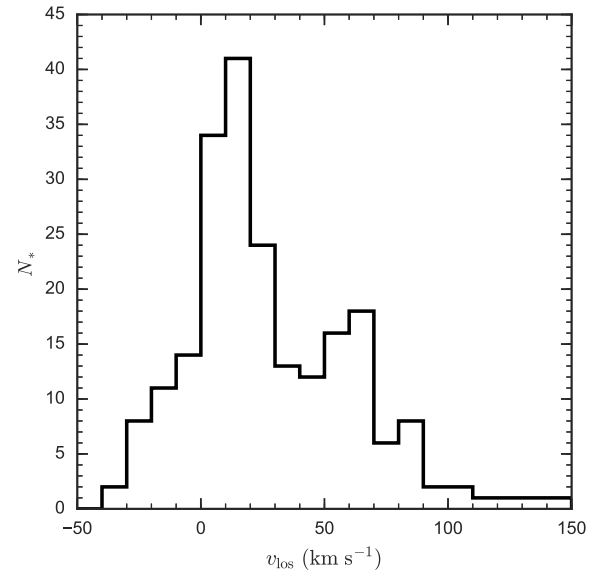


Figure 2. Histogram of line of sight for stars in the $(l, b) = (270^\circ, 0)$ APOGEE-2S field. The distribution displays a clear secondary peak.

a final sample of 215 stars with distance estimates, with a median distance uncertainty of 357 pc. This may be underestimated owing to the uncertainty in $\log g$. However, Bovy (2010) shows that the secondary peak of Hercules remains clearly visible with distance errors of 30 per cent, so the relative distance error of 10–20 per cent expected here should be sufficient for this analysis.

3 EXPECTATION FROM GALACTIC MODELS

To compare the data to the competing resonance models discussed in the introduction, we make predictions for the observed line-of-sight velocity distribution in this section. In Section 3.1, we describe how we make detailed predictions using the formalism of Dehnen (2000) and Bovy (2010) for the model where the Hercules feature represents the effect of the OLR. In Section 3.2, we discuss how we extract predictions for the slow-bar model from the work of Pérez-Villegas et al. (2017).

3.1 The fast bar

To make predictions for the fast-bar model, which is capable of reproducing the Hercules stream in the solar neighbourhood through the OLR (Dehnen 2000), we use `galpy`¹ (Bovy 2015) to simulate the orbits of stars along the $(l, b) = (270^\circ, 0)$ line of sight. Because all of the stars in our sample are close to the Galactic mid-plane, we only simulate the two-dimensional dynamics in the Galactic plane, ignoring vertical motions. To represent the distribution of stellar orbits, we use a Dehnen distribution function (Dehnen 1999) to model the stellar disc before bar formation. This distribution function (DF) is a function of energy E and angular momentum L

$$f_{\text{Dehnen}}(E, L) \propto \frac{\Sigma(R_e)}{\sigma_R^2(R_e)} \exp \left[\frac{\Omega(R_e)[L - L_c(E)]}{\sigma_R^2(R_e)} \right], \quad (2)$$

where R_e , $\Omega(R_e)$ and L_c are the radius, angular frequency and angular momentum, respectively, of the circular orbit with energy E .

¹ Available at <https://github.com/jobovy/galpy>.

The gravitational potential is assumed to be a simple power law, such that the circular velocity is given by

$$v_c(R) = v_0(R/R_0)^\beta, \quad (3)$$

where v_0 is the circular velocity at the solar circle at radius R_0 . To model the bar we use the simple quadrupole bar potential from Dehnen (2000) given by

$$\Phi(R, \phi) = A_b(t) \cos(2(\phi - \Omega_b t)) \times \begin{cases} -(R_b/R)^3, & \text{for } R \geq R_b, \\ (R/R_b)^3 - 2, & \text{for } R \leq R_b, \end{cases} \quad (4)$$

where R_b is the bar radius, set to 80 per cent of the corotation radius. The bar is grown smoothly following the prescription

$$A_b(t) = \begin{cases} 0, & t/T_b < t_1 \\ A_f \left[\frac{3}{16}\xi^5 - \frac{5}{8}\xi^3 + \frac{15}{16}\xi + \frac{1}{2} \right], & t_1 \leq t/T_b \leq t_1 + t_2 \\ A_f, & t/T_b > t_1 + t_2, \end{cases} \quad (5)$$

where t_1 is the start of bar growth, set to half the integration time, and t_2 is the duration of the bar growth. $T_b = 2\pi/\Omega_b$ is the period of the bar,

$$\xi = 2 \frac{t/T_b - t_1}{t_2} - 1, \quad (6)$$

and

$$A_f = \alpha \frac{v_0^2}{3} \left(\frac{R_0}{R_b} \right)^3, \quad (7)$$

where α is the dimensionless strength of the bar. For our fast-bar model, we set $\alpha = 0.01$, $R_0 = 8.0$ kpc and $v_0 = 220$ km s⁻¹.

Following Dehnen (2000) we specify the final time t_2 , and integrate backwards to $t = 0$. This is valid because the potential is known, and the DF remains constant along stellar orbits, as known from the collisionless Boltzmann equation. Thus, the value of the DF $f(\mathbf{r}, t_2)$ for some phase space coordinates $\mathbf{r} = (\mathbf{x}, \mathbf{v})$ at t_2 is equal to $f(\mathbf{r}_0, 0)$ if \mathbf{r} is the result of integrating \mathbf{r}_0 from $t = 0$ to $t = t_2$. Therefore, we can obtain \mathbf{r}_0 by integrating the orbits backwards in time.

The fiducial model from Dehnen (2000) and that explored in detail by Bovy (2010) had a flat rotation curve ($\beta = 0$) and OLR radius of $R_{\text{OLR}} = 0.9 R_0$. We slightly adjust these parameters to provide a better match to the data in Section 4: $R_{\text{OLR}} = 0.95 R_0$ and $\beta = -0.1$ (a slightly falling rotation curve). This change causes the separation of the Hercules feature from the main mode of the velocity distribution to be slightly smaller. We combine this gravitational-potential model with a Dehnen distribution function appropriate for the kinematics of the APOGEE sample of intermediate-age stars (Bovy et al. 2012): surface-density scalelength $R_0/3$ and an exponential radial velocity dispersion with scalelength R_0 and $\sigma_R(R_0) = 33$ km s⁻¹. The bar has an angle of 25° with respect to the Sun–Galactic Centre line, a pattern speed of $\Omega_b = 48.6$ km s⁻¹ kpc⁻¹ and corotation occurs at $R_{\text{CR}} = 4.77$ kpc.

Fig. 3 displays the local velocity (U, V) distribution in the solar neighbourhood for our chosen bar parameters, where U is the velocity in the direction of the Galactic Centre and V is the velocity in the direction of rotation with respect to the local standard of rest (LSR). It clearly reproduces a Hercules-like bimodality, with the density peak of the Hercules feature occurring around $U = -30$ km s⁻¹ with respect to the LSR, or $U = -40$ km s⁻¹ with respect to the Sun, which is in agreement with the literature (e.g. Dehnen 1998; Famaey et al. 2005; Bovy, Hogg & Roweis 2009; Pérez-Villegas

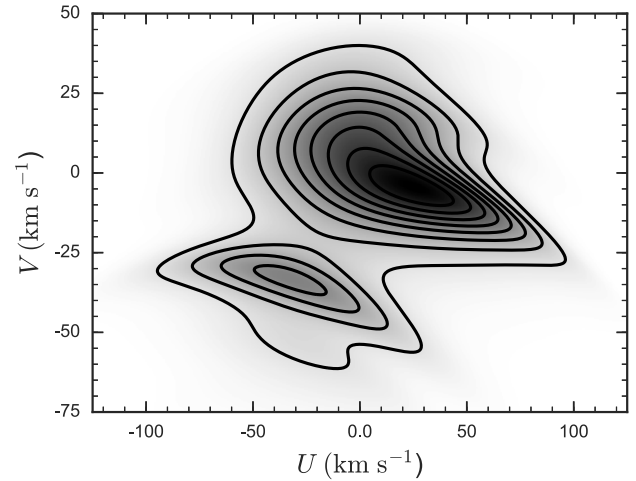


Figure 3. The velocity distribution in the solar neighbourhood for the fast-bar model from Section 3.1 for the chosen model parameters.

et al. 2017). We do not expect this simple model to well reproduce the main density peak of the solar neighbourhood, which is heavily influenced by other non-axisymmetric components and dynamical processes such as the spiral structure and other moving groups.

Below we also compare the data to a simple axisymmetric model. This model is that of this section, except that it has no bar.

3.2 The slow bar

To make predictions for the slow bar, which can reproduce a Hercules-like feature in the velocity distribution in the solar neighbourhood through orbits around the bar’s Lagrange points, we examine the velocity distribution of the model from Pérez-Villegas et al. (2017). We do this rather than evaluating a simple model like that for the fast bar described above, because simple models for the slow bar do not reproduce the Hercules stream in the solar neighbourhood (Monari et al. 2017a). The model is based on the Made-to-Measure (e.g. Syer & Tremaine 1996; de Lorenzi et al. 2007; Hunt & Kawata 2014) model from Portail et al. (2017a) which reproduces a range of observational constraints in the bulge and bar region. In this model, the bar has a pattern speed of $\Omega_b = 39$ km s⁻¹ kpc⁻¹, with an angle of 28° with respect to the Sun–Galactic Centre line. The Sun is located at $R_0 = 8.2$ kpc, and the local circular velocity $v_c(R_0) = 243$ km s⁻¹.

The effective potential of the bar is constrained by the fitted bulge-bar data, and therefore the perturbations and resonant orbits in the outer disc are predicted. However, the population of these orbits and the DF in the outer disc is not fitted. Pérez-Villegas et al. (2017) adjust the model from Portail et al. (2017a) by increasing the resolution by a factor of 10, following a variation of the resampling scheme presented in Dehnen (2009). Because no data were fitted in the outer disc of this model, the velocity dispersion of the disc was unconstrained and depends heavily on the initial N -body model which was hotter than the Milky Way’s disc. Therefore, Pérez-Villegas et al. (2017) cooled the outer disc to $\sigma_R = 35.5$ km s⁻¹ to reproduce the local radial velocity dispersion. However, it is clear from fig. 2 of that work that even this cooled disc is too hot to reproduce the rich and complex substructure in the UV diagram. Fitting the model to this local velocity distribution is currently infeasible because it would require knowledge of the presently ill constrained potential of the spiral arms. Therefore, we compare the model of Pérez-Villegas et al. (2017) as it is, selecting

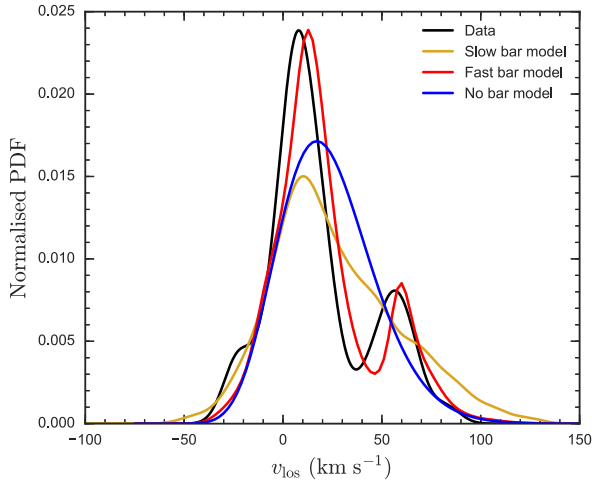


Figure 4. KDE of the data in the range $2.2 \leq d \leq 3.2$ kpc (black) overlaid with the axisymmetric prediction (blue), the fast-bar model prediction (red) and the slow-bar model (gold).

particles in a 100 pc cylinder along the $(l, b) = (270^\circ, 0)$ line of sight assuming $R_0 = 8.2$ kpc following the model.

4 COMPARISON WITH DATA

Fig. 4 shows a Kernel Density Estimate (KDE; Wasserman 2006) with bandwidth 7 km s^{-1} of the observed line-of-sight velocity distribution (black) in the range $2.2 \leq d \leq 3.2$ kpc, chosen for being the range where the feature appears to be strongest in the data. We compare the data distribution to the prediction from the short bar model (red) and a KDE prediction from slow-bar model both computed at the same distance. We also include the prediction from a

simple axisymmetric for reference; this is not expected to reproduce the Hercules peak.

Note that Pérez-Villegas et al. (2017) assume a solar motion of 12.24 km s^{-1} (Schönrich, Binney & Dehnen 2010). We remind the reader that in this work we compare the models and data in the local standard of rest frame having corrected the data by 24 km s^{-1} . A different solar motion would shift the observed velocity distribution without changing its shape.

There is excellent agreement between the fast-bar model prediction and the data, except for a 4 km s^{-1} misalignment of the peaks, which could be due to a slight overestimation of the solar velocity. The slow-bar model is clearly too hot compared to the data. This is already known from the comparison to the solar neighbourhood *UV* plot in Pérez-Villegas et al. (2017); the larger width of the main peak is owing to the high dispersion, not the orbital origin of Hercules. The slow-bar model does not have a clear Hercules-like peak, unlike the data and the fast-bar model. However, note that the model was not fitted to reproduce the velocity distribution in the outer disc, aside from cooling it to better reproduce the local velocity dispersion. It was fitted to the entire bar region, which naturally produces a feature consistent with Hercules in the solar neighbourhood.

Fig. 5 displays the histogram of the line-of-sight velocity distribution for the data in black for six 500 pc wide distance bins between 1 and 4 kpc. These histograms show that a clear second peak is present in the data in the three bins between 1.5 and 3 kpc. We also overlay the predictions for the axisymmetric, fast-bar and slow-bar models. For the distance bins under 3 kpc, the fast-bar model shows an excellent match to the data. The distance bins over 3 kpc have comparatively few stars, and it is hard to distinguish between the axisymmetric and both bar models which all fit the data well. Qualitatively, the slow-bar model can populate the area of the distribution containing the Hercules stream. However, there is no clear division between the central peak and Hercules in the slow-bar

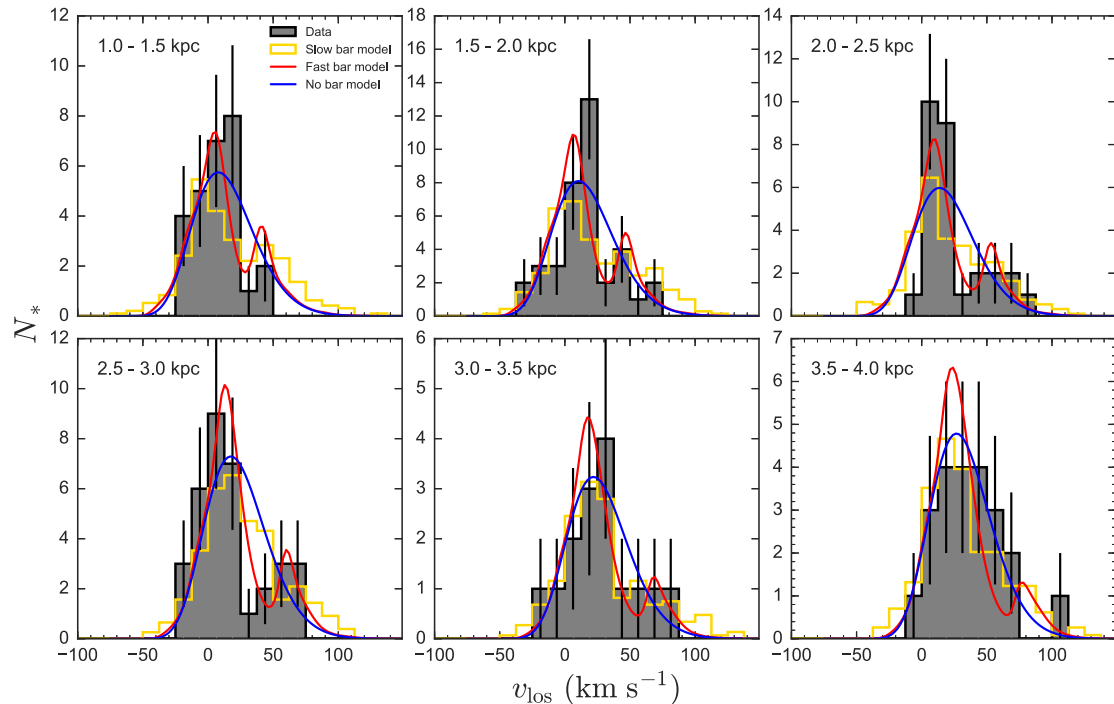


Figure 5. Histogram of the line-of-sight velocity distribution (km s^{-1}) for the data (black) overlaid with the prediction from an axisymmetric model (blue), the fast-bar model (red) and the slow-bar model (gold) for six distance bins in the range 1–4 kpc. The error bars show the Poisson errors for the data. All three models have been normalized to match the number counts in the data.

model. It is difficult to say whether this is an intrinsic feature of the mechanism which populates the orbit space, or a result of the high velocity dispersion.

5 DISCUSSION AND OUTLOOK

We have shown that there is a bimodality in the line-of-sight velocity distribution in data taken by APOGEE-2S along $(l, b) = (270^\circ, 0)$ up to around 4 kpc, matching the expected location of the Hercules stream. This is substantially further from the Sun than any existing detection of the Hercules stream. It leaves no doubt that the Hercules stream is indeed a large-scale dynamical feature in the Milky Way, rather than a localized solar-neighbourhood anomaly.

The stream can plausibly be explained as the effect of OLR of a short, fast-rotating Galactic bar (Dehnen 2000), or as the result of stars orbiting the Lagrange points of a long slower rotating Galactic bar (Pérez-Villegas et al. 2017). We compared the observed velocity distribution with predictions from the two models around a distance of 2.7 kpc where the feature was strongest in the data. We find that the fast-bar model is an excellent match to the data, while the slow-bar model does not reproduce two clearly divided modes. We also compared the data with the models in six separate distance bins from 1 to 4 kpc. Again we find that the fast-bar model is a better match. The slow-bar model consistently populates the area of the distribution containing the Hercules stream, but without the observed bimodal structure. This could be owing to the high velocity dispersion obscuring any separation between the modes, and thus future work is necessary to better predict the expected velocity distribution in the slow-bar model for the APOGEE sample.

We also note here that we do not find that the stars in the Hercules stream have systematically higher metallicity than the sample in general. This is in agreement with Bovy & Hogg (2010), who find no significant metallicity preference in Hercules in the solar neighbourhood, but in conflict with Raboud et al. (1998) who report the anomaly in the (U, V) plane (Hercules) to consist of intermediate to high metallicity stars.

In the near future, *Gaia* will provide 5D phase space information for over 10^9 stars down to ~ 20 mag, and radial velocities for around 10^8 stars down to ~ 16 mag. The brightest stellar types will be visible across many kpc, enabling us to trace the extent of Hercules in all directions and also refine our measurements of the extent of the Galactic bar. At this stage it should become clear whether the Hercules stream conforms to the OLR explanation for its origin, or whether another mechanism is required to explain the observed velocity distribution across the disc.

ACKNOWLEDGEMENTS

We thank the anonymous referee for their valuable comments. We would like to thank Alexey Mints for valuable help with the UNIDAM code. JASH is supported by a Dunlap Fellowship at the Dunlap Institute for Astronomy & Astrophysics, funded through an endowment established by the Dunlap family and the University of Toronto. JB received partial support from the Natural Sciences and Engineering Research Council of Canada. JB also received partial support from an Alfred P. Sloan Fellowship. RRL acknowledges support by the Chilean Ministry of Economy, Development and Tourism's Millennium Science Initiative through grant IC120009, awarded to The Millennium Institute of Astrophysics (MAS). RRL also acknowledges support from the STFC/Newton Fund ST/M007995/1 and the CONICYT/Newton Fund DPI20140114. PLP was supported by MINEDUC-UA project, code ANT 1655.

Funding for the Sloan Digital Sky Survey IV has been provided by the Alfred P. Sloan Foundation, the U.S. Department of Energy Office of Science and the Participating Institutions. SDSS-IV acknowledges support and resources from the Center for High-Performance Computing at the University of Utah. The SDSS web site is www.sdss.org.

SDSS-IV is managed by the Astrophysical Research Consortium for the Participating Institutions of the SDSS Collaboration including the Brazilian Participation Group, the Carnegie Institution for Science, Carnegie Mellon University, the Chilean Participation Group, the French Participation Group, Harvard-Smithsonian Center for Astrophysics, Instituto de Astrofísica de Canarias, The Johns Hopkins University, Kavli Institute for the Physics and Mathematics of the Universe (IPMU)/University of Tokyo, Lawrence Berkeley National Laboratory, Leibniz Institut für Astrophysik Potsdam (AIP), Max-Planck-Institut für Astronomie (MPIA Heidelberg), Max-Planck-Institut für Astrophysik (MPA Garching), Max-Planck-Institut für Extraterrestrische Physik (MPE), National Astronomical Observatories of China, New Mexico State University, New York University, University of Notre Dame, Observatório Nacional/MCTI, The Ohio State University, Pennsylvania State University, Shanghai Astronomical Observatory, United Kingdom Participation Group, Universidad Nacional Autónoma de México, University of Arizona, University of Colorado Boulder, University of Oxford, University of Portsmouth, University of Utah, University of Virginia, University of Washington, University of Wisconsin, Vanderbilt University and Yale University.

REFERENCES

- Antoja T. et al., 2014, *A&A*, 563, A60
 Bensby T., Oey M. S., Feltzing S., Gustafsson B., 2007, *ApJ*, 655, L89
 Blanton M. R. et al., 2017, *AJ*, 154, 28
 Blitz L., Spergel D. N., 1991, *ApJ*, 379, 631
 Bovy J., 2010, *ApJ*, 725, 1676
 Bovy J., 2015, *ApJS*, 216, 29
 Bovy J., Hogg D. W., 2010, *ApJ*, 717, 617
 Bovy J., Hogg D. W., Roweis S. T., 2009, *ApJ*, 700, 1794
 Bovy J. et al., 2012, *ApJ*, 759, 131
 Bovy J., Bird J. C., García Pérez A. E., Majewski S. R., Nidever D. L., Zasowski G., 2015, *ApJ*, 800, 83
 Bowen I. S., Vaughan A. H., Jr, 1973, *Appl. Opt.*, 12, 1430
 Bressan A., Marigo P., Girardi L., Salasnich B., Dal Cero C., Rubele S., Nanni A., 2012, *MNRAS*, 427, 127
 Cabrera-Lavers A., González-Fernández C., Garzón F., Hammersley P. L., López-Corredoira M., 2008, *A&A*, 491, 781
 Contopoulos G., 1980, *A&A*, 81, 198
 de Lorenzi F., Debattista V. P., Gerhard O., Sambhus N., 2007, *MNRAS*, 376, 71
 de Vaucouleurs G., 1964, in Kerr F. J., ed. *IAU Symp. 20, The Galaxy and the Magellanic Clouds*. Australian Acad. Sci., Canberra, p. 195
 Dehnen W., 1998, *AJ*, 115, 2384
 Dehnen W., 1999, *AJ*, 118, 1201
 Dehnen W., 2000, *AJ*, 119, 800
 Dehnen W., 2009, *MNRAS*, 395, 1079
 Famaey B., Jorissen A., Luri X., Mayor M., Udry S., Dejonghe H., Turon C., 2005, *A&A*, 430, 165
 Gaia Collaboration, 2016a, *A&A*, 595, A1
 Gaia Collaboration, 2016b, *A&A*, 595, A2
 García Pérez A. E. et al., 2016, *AJ*, 151, 144
 Gunn J. E. et al., 2006, *AJ*, 131, 2332
 Holtzman J. A. et al., 2015, *AJ*, 150, 148
 Hunt J. A. S., Kawata D., 2014, *MNRAS*, 443, 2112
 Liu C., Xue X., Fang M., van de Ven G., Wu Y., Smith M. C., Carrell K., 2012, *ApJ*, 753, L24

- Majewski S. R., APOGEE Team, APOGEE-2 Team, 2016, *Astron. Nachr.*, 337, 863
- Majewski S. R. et al., 2017, *AJ*, 154, 94
- McWilliam A., Zoccali M., 2010, *ApJ*, 724, 1491
- Minchev I., Nordhaus J., Quillen A. C., 2007, *ApJ*, 664, L31
- Minchev I., Boily C., Siebert A., Bienayme O., 2010, *MNRAS*, 407, 2122
- Mints A., Hekker S., 2017, *A&A*, 604, A108
- Monari G., Famaey B., Siebert A., Duchateau A., Lorscheider T., Bienaymé O., 2017a, *MNRAS*, 465, 1443
- Monari G., Kawata D., Hunt J. A. S., Famaey B., 2017b, *MNRAS*, 466, L113
- Nataf D. M., Udalski A., Gould A., Fouqué P., Stanek K. Z., 2010, *ApJ*, 721, L28
- Ness M. et al., 2016, *ApJ*, 819, 2
- Nidever D. L. et al., 2015, *AJ*, 150, 173
- Pérez-Villegas A., Portail M., Wegg C., Gerhard O., 2017, *ApJ*, 840, L2
- Portail M., Gerhard O., Wegg C., Ness M., 2017a, *MNRAS*, 465, 1621
- Portail M., Wegg C., Gerhard O., Ness M., 2017b, *MNRAS*, 470, 1233
- Raboud D., Grenon M., Martinet L., Fux R., Udry S., 1998, *A&A*, 335, L61
- Schönrich R., Binney J., Dehnen W., 2010, *MNRAS*, 403, 1829
- Steinmetz M. et al., 2006, *AJ*, 132, 1645
- Syer D., Tremaine S., 1996, *MNRAS*, 282, 223
- Wasserman L., 2006, *All of Nonparametric Statistics* (Springer Texts in Statistics). Springer-Verlag New York, Inc., Secaucus, NJ, USA
- Wegg C., Gerhard O., Portail M., 2015, *MNRAS*, 450, 4050
- Williams A. A. et al., 2016, *ApJ*, 824, L29
- Wilson J. C. et al., 2010, in *Proc. SPIE Conf. Ser. Vol. 7735, Ground-based and Airborne Instrumentation for Astronomy III*. SPIE, Bellingham, p. 77351C
- Zasowski G. et al., 2017, *AJ*, 154, 198
- Zhao G., Zhao Y.-H., Chu Y.-Q., Jing Y.-P., Deng L.-C., 2012, *Res. Astron. Astrophys.*, 12, 723

This paper has been typeset from a $\text{\TeX}/\text{\LaTeX}$ file prepared by the author.